Dynamic Analysis of a Geometrical Non-Linear Plate Using the Continuous-Time System Identification

Jae-Hoon Lim
School of Mechanical Engineering, Sungkyunkwan University, 300, Chunchun-dong, Jangan-gu, Suwon, Kyunggi-do 440-746, Korea
Yeon-Sun Choi*
School of Mechanical Engineering, Sungkyunkwan University, 300, Chunchun-dong, Jangan-gu, Suwon, Kyunggi-do 440-746, Korea

The dynamic analysis of a plate with non-linearity due to large deformation was investigated in this study. There have been many theoretical and numerical analyses of the non-linear dynamic behavior of plates examining theoretically or numerically. The problem is how correctly an analytical model can represent the dynamic characteristics of the actual system. To address the issue, the continuous-time system identification technique was used to generate non-linear models, for stiffness and damping terms, and to explain the observed behaviors with single mode assumption after comparing experimental results with the numerical results of a linear plate model.

Key Words : Geometrical Nonlinear, Plate, System Identification, Nonlinear Damping, Bifurcation

1. Introduction

The dynamic analysis of plates gained importance with the development of mechanics theory. There are several linear theories of plates such as the two dimensional approximation of Euler-Bernoulli beam and the Mindlin plate theory of Timoshenko beam model. Plates, however, are generally subject to an out-of-plane or in-plane excitation, which causes a nonlinear behavior of the system. That is, there are the bending stress and the stress according to a tensile strain in the membrane due to a large deformation (Timoshenko and Woinowsky-Kreiger, 1959). These stresses lead to a geometrical non-linearity of the plate. Many of the most compelling studies were on the geometrical non-linear vibration of plates. Some of the studies were based on non-linearity such as shear strain or curvature with large deformation. Gorman (1995) derived analytically homogeneous solutions of the cantilevered rectangular plate by means of the building block superposition method. Also, he examined the eigenvalues of the plate along the variance of the orthotropic parameters and the length ratio between horizontal and vertical line. Kadiri (Kadiri et al., 1999) calculated the non-linear mode of the fixed rectangular plate due to large deformation using Hamilton's principle and the spectral analysis. Haterbouch (Haterbouch and Benamar, 2003) examined the effect of the large deformation of a fixed circular plate on the first two line symmetry mode shapes, natural frequencies and distributed bending stress. He derived a nonlinear equation of motion of circular plate using Hamilton's principle and Bessel function. Then he induced nonlinear mode shapes and non-linear natural frequencies. The researches on such a non-

* Corresponding Author,
E-mail : yschoi@yurim.skku.ac.kr
TEL : +82-31-290-7440; **FAX** : +82-31-290-5889
School of Mechanical Engineering, Sungkyunkwan University, 300, Chunchun-dong, Jangan-gu, Suwon, Kyunggi-do 440-746, Korea. (Manuscript **Received** November 17, 2005; **Revised** July 31, 2006)

linear plate have mainly dealt with proposing an analytical model or a procedure for obtaining a numerical solution. In the non-linear system, however, a correlation between a non-linear equation and the response of the actual system is no less important than the proposed equation. It is necessary to prove with experimental data whether an analytical model reflects the actual system. Accordingly, a system identification method and a single mode approximation were used in this study to estimate the parameters of the nonlinear terms with experimental data after establishing theoretically a geometrical non-linear dynamic equation.

2. Natural Frequencies of the Plate

To analyze the behavior of a plate the equation of motion of the cantilevered rectangular plate shown in Fig. 1 was induced. Considering the plate with the lengths a and b along the x, y directions, respectively, a thickness h, Young's modulus E and Poisson ratio ν. The plate was clamped at $x=0$, $0\le y\le b$ and a distributed mass with the thickness h', which was attached at $a_0\le x\le a$, $0\le y\le b$ to convert an exciting force $F(t)$ at $x=x_0$, $y=y_0$ into a line force as shown in Fig. 1.

The shear deformation and rotary inertia of the plate were neglected and it was assumed that the plate was isotropic and homogeneous satisfying the Hooke's law. The equation of motion of the plate containing the distributed mass is as follows (Wong, 2002)

$$-\nabla^4(Dz(x,y,t))+F(x_0,y_0,t)=\frac{\partial^2(\rho habz(x,y,t))}{\partial t^2}+\frac{\partial^2(\rho h'Az(x,y,t))}{\partial t^2} \quad (1)$$

where, the flexural rigidity of the plate is $D=Ebh^3/12(1-\nu^2)$, ∇^4 is a biharmonic operator and A is the area of the distributed mass, $A=(a-a_0)\times b$.

First, to obtain the natural frequencies of the plate let us assume the solution of Eq. (1) to be Eq. (2).

$$z(x,y,t)=\sum_n\sum_m A_{nm}\phi_n(x)\,\psi_m(y)\sin\omega t \quad (2)$$

where, $\phi_n(x)$, $\psi_m(y)$ are the eigenfunctions of beams, which satisfy the boundary condition of x, y direction, respectively. Also, the maximum potential and kinetic energy are as in the Eq. (3).

$$U_{\max}=\frac{D}{2}\left\{\int_0^a\int_0^b\left(\left(\frac{\partial^2W}{\partial x^2}\right)^2+\left(\frac{\partial^2W}{\partial y^2}\right)^2\right)dxdy+\int_0^a\int_0^b\left(2\nu\frac{\partial^2W}{\partial x^2}\frac{\partial^2W}{\partial y^2}\right)dxdy+\int_0^a\int_0^b\left(2(1-\nu)\frac{\partial^2W}{\partial x\partial y}\right)dxdy\right\} \quad (3)$$

$$T_{\max}=\frac{\rho h\omega^2}{2}\int_0^a\int_0^b W^2dxdy+\frac{\rho h'\omega^2}{2}\int_{a_0}^a\int_0^b W^2dxdy$$

$$W(x,y)=\sum_n\sum_m A_{nm}\phi_n(x)\,\psi_m(y)$$

Substituting $W(x,y)$ into $U_{\max}$ and $T_{\max}$ and utilizing the Rayleigh-Ritz method, algebraic equations were obtained as illustrated in Eq. (4).

$$\begin{aligned}&\sum_n\sum_m\left\{\int_0^a\left(\frac{d^2\phi_m}{dx^2}\right)\left(\frac{d^2\phi_i}{dx^2}\right)dx\int_0^b\psi_n\psi_j dy\right.\\&+\int_0^a\phi_m\phi_i dx\int_0^b\left(\frac{d^2\psi_n}{dy^2}\right)\left(\frac{d^2\psi_j}{dy^2}\right)dy\\&+\nu\left[\int_0^a\phi_m\left(\frac{d^2\phi_i}{dx^2}\right)dx\int_0^b\left(\frac{d^2\psi_n}{dy^2}\right)\psi_j dy\right.\\&\left.+\int_0^a\left(\frac{d^2\phi_m}{dx^2}\right)\phi_i dx\int_0^b\psi_n\left(\frac{d^2\psi_j}{dy^2}\right)dy\right]\\&+2(1-\nu)\left[\int_0^a\left(\frac{d\phi_m}{dx}\right)\left(\frac{d\phi_i}{dx}\right)dx\int_0^b\left(\frac{d\psi_n}{dy}\right)\left(\frac{d\psi_j}{dy}\right)dy\right]\\&-\lambda\left[\int_0^a\phi_m\phi_i dx\int_0^b\psi_n\psi_j dy\right.\\&\left.\left.+(h'/h)\int_{a_0}^a\phi_m\phi_i dx\int_0^b\psi_n\psi_j dy\right]\right\}A_{mn}=0\end{aligned} \quad (4)$$

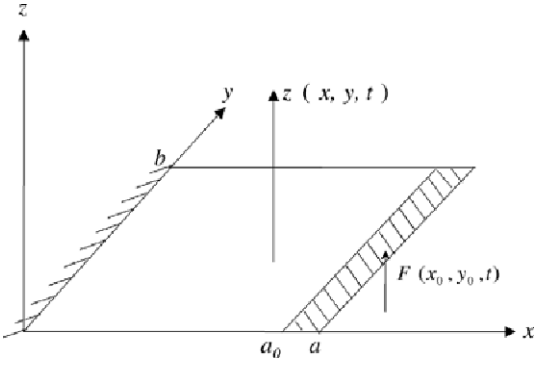

Fig. 1 Schematic of the plate

where, $\lambda=\rho h\omega^2/D$ and m, n, i, $j=1, 2, 3, \cdots, N$. From Eq. (4) the natural frequencies can be calculated.

The experimental set up shown in Fig. 2 was used to investigate the plates. The produced plate properties and design variables are represented in Table 1. To obtain the natural frequencies of the plate experimentally, a modal analysis was conducted by means of the impact test. The frequency response functions were measured from the responses obtained by an accelerometer (B&K 4371) after exciting the plate by an impact hammer (B&K 8202). The measuring process consisted of an excitation at a definite point and measurements at the other points. Also, each experiment was repeated over 16 times and the data averaged in order to decrease the noise that occurred during the experiment and, increase data reliability.

The SMS (Spectral dynamics Co., 1994) software was utilized to calculate the natural frequencies and the mode shapes of the plate with the measured frequency response functions. With the FE-analysis program, Samcef (Samtech Co., 2003), comparisons were made between the numerical data and experimental results. The first three mode shapes from the numerical and experimental results are depicted in Fig. 3. Also, the natural frequencies from the experiments, FE and theoretical analyses using Eq. (5) are represented in Table 2.

$$z(x,y,t)=\sum_{n,m,i} W_{n,m}(x,y)\,q_i(t)$$
$$W_{n,m}(x,y)=\phi_n(x)\,\psi_m(y) \tag{5}$$

where, $q_i(t)$ is the generalized coordinate, modal displacement, and $\phi_n(x)$, $\psi_m(y)$ are the eigenfunctions of the beam as mentioned above. With the data from each point, each modal displacement of q_1, q_2, and q_3, were obtained using Eq. (6).

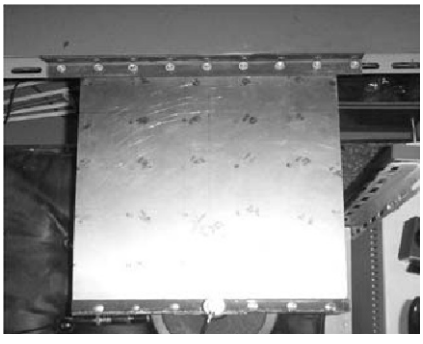

Fig. 2 Experimental set-up

Table 1 Properties of the plate

E, Young's modulus	200 GPa
ρ, density	7850 kg/m^3
ν, Poisson's ratio	0.3
a, b, lengths	0.32, 0.3 m
h, thickness	0.0007 m
h', thickness of distributed mass	0.005 m
$a-a_0$, b, lengths of distributed mass	0.01, 0.3 m

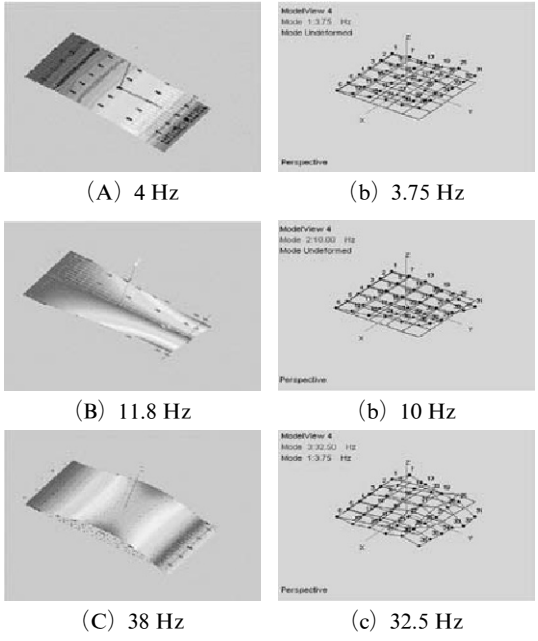

(A) 4 Hz (b) 3.75 Hz

(B) 11.8 Hz (b) 10 Hz

(C) 38 Hz (c) 32.5 Hz

Fig. 3 Vibration modes of the plate; (A), (B) and (C) by Samcef, (a), (b) and (c) by SMS

Table 2 Natural frequencies of the plate with different methods

natural frequency	FE-analysis	theoretical	experimental
ω_1	4 Hz	4.47 Hz	3.75 Hz
ω_2	11.8 Hz	12.33 Hz	10 Hz
ω_3	38 Hz	39.1 Hz	32.5 Hz

$$\begin{bmatrix} q_1(t_1) & \cdots & q_1(t_N) \\ q_2(t_1) & \cdots & q_2(t_N) \\ q_3(t_1) & \cdots & q_3(t_N) \end{bmatrix} = \begin{bmatrix} W_{1,1}(a_1,b_1) & W_{1,2}(a_1,b_1) & W_{2,1}(a_1,b_1) \\ W_{1,1}(a_2,b_2) & W_{1,2}(a_2,b_2) & W_{2,1}(a_2,b_2) \\ W_{1,1}(a_3,b_3) & W_{1,2}(a_3,b_3) & W_{2,1}(a_3,b_3) \end{bmatrix}^{-1} \begin{bmatrix} z(a_1,b_1,t_1) & \cdots & z(a_1,b_1,t_N) \\ z(a_2,b_2,t_1) & \cdots & z(a_2,b_2,t_N) \\ z(a_3,b_3,t_1) & \cdots & z(a_3,b_3,t_N) \end{bmatrix} \quad (6)$$

$W_{1,1}$, $W_{1,2}$, $W_{2,1}$ can be determined from the previous theoretical modal analysis. Figs. 5 to 7 show the power spectrum and the phase diagram of each modal displacement.

Figure 5 shows that two or more periodic motions in the behavior of the first modal displacement could be observed because of the increment of the exciting frequency, which resulted in sub-harmonic components of the exciting frequency in the frequency spectrum. Furthermore, there was a chaotic-like motion at 55 Hz. The frequency spectra and the phase diagrams of the second modal displacement are depicted in Fig. 6. Fig. 6 shows that two or more periodic motion and a chaotic-like motion also occurred beyond the exciting frequency of 22 Hz. In Fig. 7, however, the Hopf bifurcation occurred over 29 Hz of the exciting frequency so that two-periodic motions were verified in the behavior of the third modal displacement. The bifurcation diagrams for each modal displacement are depicted in Fig. 8.

Meanwhile, to compare experimental data with the results from the linear analyses, the solutions of Eq. (1) were assumed to be Eq. (5), and the

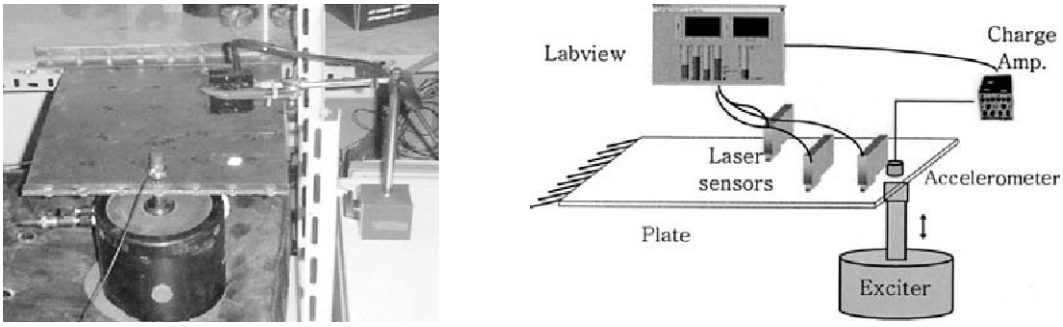

(a) The plate with an exciter (b) Schematics of the experimental system

Fig. 4 Experimental apparatus

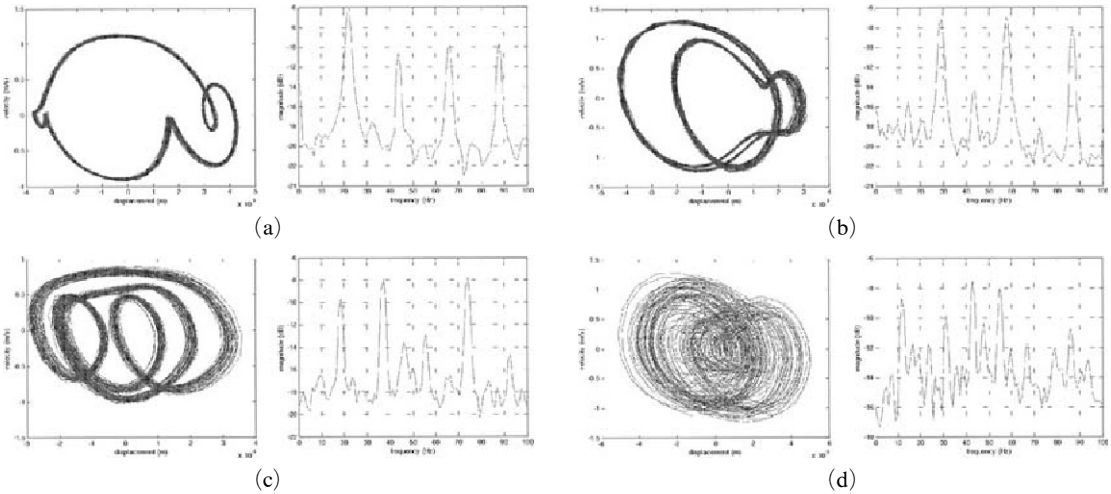

Fig. 5 Phase diagrams and power spectra of the first modal responses for ; (a) 22 Hz, (b) 29 Hz, (c) 37 Hz and (d) 55 Hz

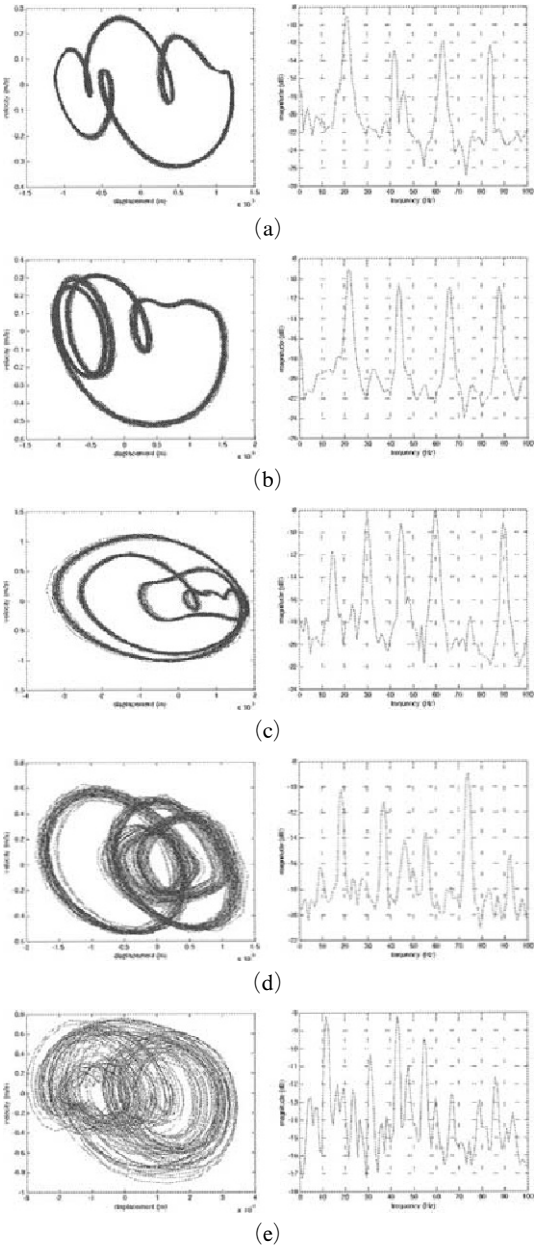

Fig. 6 Phase diagrams and power spectra of the second modal responses for ; (a) 21 Hz, (b) 22 Hz, (c) 30 Hz, (d) 37 Hz and (e) 55 Hz

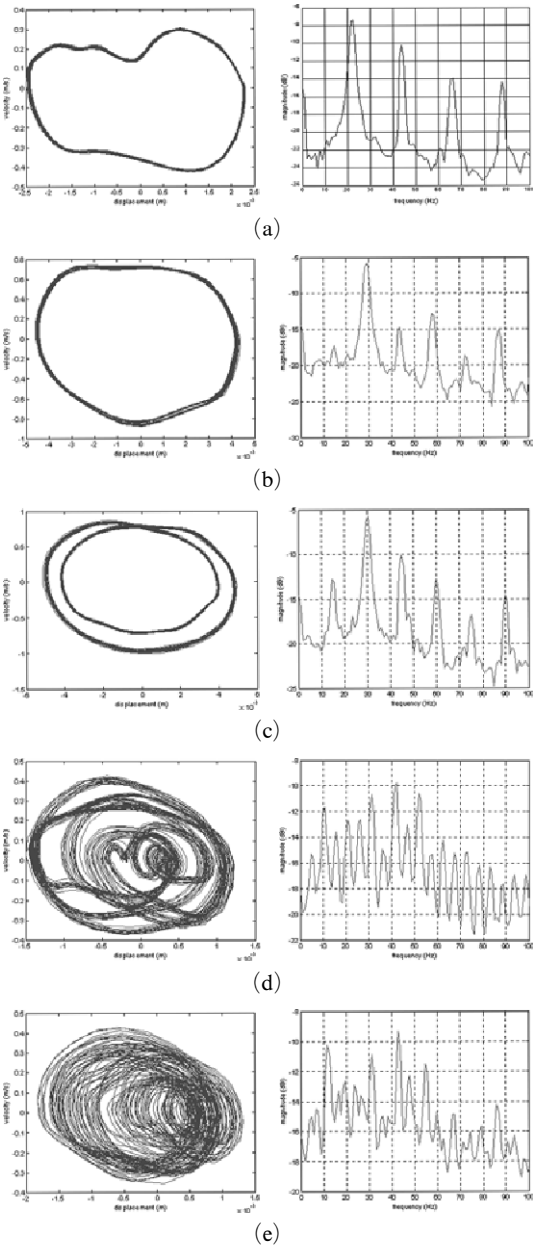

Fig. 7 Phase diagrams and power spectra of the third modal responses for ; (a) 22 Hz, (b) 29 Hz, (c) 30 Hz, (d) 52 Hz and (e) 55 Hz

Galerkin's method for the separation of variables was applied. The results from the experimental excitation data are depicted in Figs. 9 and 10. As shown in Figs. 9 and 10, there were no sub-harmonic components of the exciting frequency leading the periodic motions in the phase diagram. Also, during the experiments, the maximum amplitude of displacement of the plate (peak to peak) was 35 mm, which is over 1/10 of the length of the plate at the constant acceleration of the force, 20 g. That is, the observed displacement was beyond the applicable range of the linear plate model.

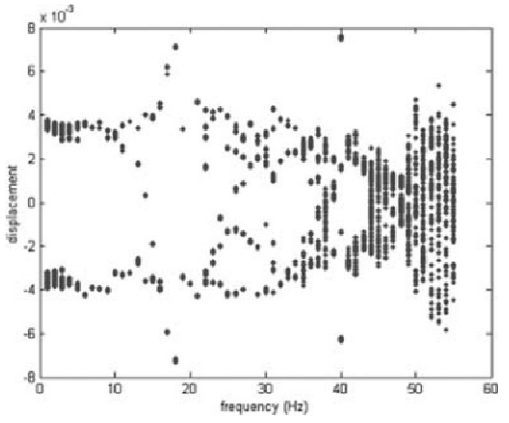

(a) The first mode

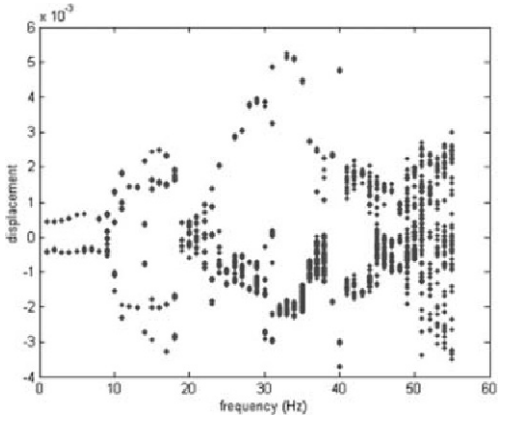

(b) The second mode

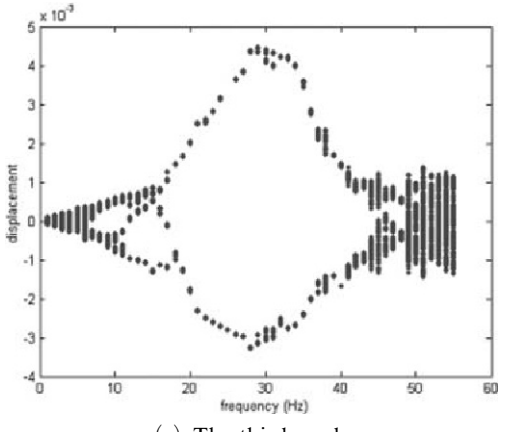

(c) The third mode

Fig. 8 Bifurcation diagram for each modal displacement

Therefore, the results from the linear plate model didn't agree with the experimental results. Consequently, the non-linear equation of motion of the plate needs to be further investigated.

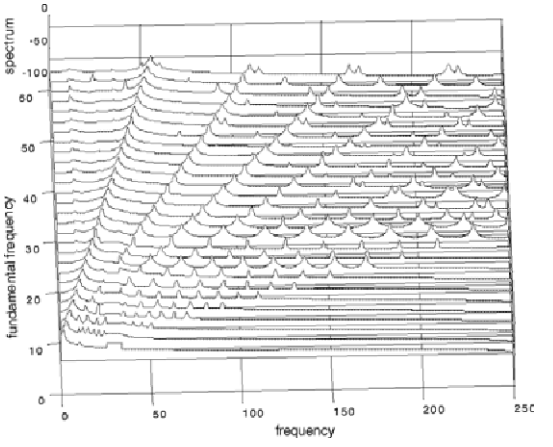

Fig. 9 Waterfall diagram of the plate spectra with linear equation of motion

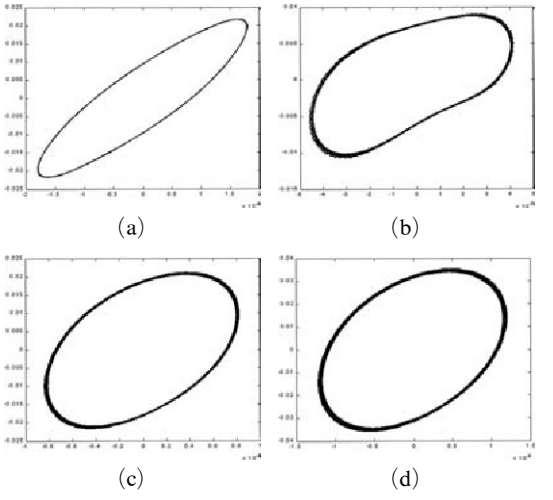

Fig. 10 Phase diagrams of the first modal displacement by numerical analysis for ; (a) 19 Hz, (b) 35 Hz, (c) 42 Hz and (d) 46 Hz

3. Non-Linear Equation of Motion of the Plate

When the deformation of a plate is larger than that of a linear assumption in a transverse vibration of a plate, a strain energy occurs in a membrane as well as a bending strain energy (Timoshenko and Woinowsky-Kreiger, 1959). Each potential energy caused by the large deformation and kinetic energy is expressed as follows (Kadiri and

Benamar, 2003).

$$
\begin{aligned}
V_b &= \frac{D}{2}\int_s \left[\left(\frac{\partial^2 z}{\partial x^2}\right)^2+\left(\frac{\partial^2 z}{\partial y^2}\right)^2\right. \\
&\quad \left.+2(1-\nu)\left(\frac{\partial^2 z}{\partial x \partial y}\right)^2+2\nu\frac{\partial^2 z}{\partial x^2}\frac{\partial^2 z}{\partial y^2}\right] ds, \\
V &= \frac{3D}{2h^2}\int_s \left[\left(\frac{\partial z}{\partial x}\right)^2+\left(\frac{\partial z}{\partial y}\right)^2\right]^2 ds, \\
T &= \frac{1}{2}\rho h\int_s \left(\frac{\partial z}{\partial t}\right)^2 ds+\frac{1}{2}\rho h'\int_A \left(\frac{\partial z}{\partial t}\right)^2 dA
\end{aligned} \tag{7}
$$

where, V_b, V_a and T are a bending potential energy, a potential energy of the membrane and a kinetic energy of the plate, respectively. The parameter s is the surface area of the plate, and A is the area of the distributed mass. Assuming the solution of the plate equation to be the expression in Eq. (8) and utilizing the Lagrange Equation with Eq. (7), one can obtain the Duffing equation of motion as shown in Eq. (9).

$$
z(x, y, t) = \sum_n \sum_m \phi_n(x)\, \psi_m(y)\, q_{nm}(t) \tag{8}
$$

$$
\begin{aligned}
& m_{ir}\ddot{q}_i + k_{ir}q_i + 2b_{ijkr}q_i q_j q_k = W_i(x_0, y_0)\, F(t), \\
& W_i(x_0, y_0) = \phi_n(x_0)\, \psi_m(y_0), \\
& m_{ir} = \rho h\left(\int_s W_i W_r ds + \frac{h'}{h}\int_A W_i W_r dA\right) \\
& k_{ir} = D\int_s \left[\frac{\partial^2 W_i}{\partial x^2}\frac{\partial^2 W_r}{\partial x^2}+\frac{\partial^2 W_i}{\partial y^2}\frac{\partial^2 W_r}{\partial y^2}\right. \\
& \quad +2(1-\nu)\frac{\partial^2 W_i}{\partial x \partial y}\frac{\partial^2 W_r}{\partial x \partial y} \\
& \quad \left.+\nu\left(\frac{\partial^2 W_i}{\partial x^2}\frac{\partial^2 W_r}{\partial y^2}+\frac{\partial^2 W_r}{\partial x^2}\frac{\partial^2 W_i}{\partial y^2}\right)\right] ds \\
& b_{ijkr} = \frac{3D}{2h^2}\int_s \left(\left(\frac{\partial W_i}{\partial x}\right)\left(\frac{\partial W_j}{\partial x}\right)+\left(\frac{\partial W_i}{\partial y}\right)\left(\frac{\partial W_i}{\partial y}\right)\right) \\
& \quad \cdot\left(\left(\frac{\partial W_k}{\partial x}\right)\left(\frac{\partial W_r}{\partial x}\right)+\left(\frac{\partial W_k}{\partial y}\right)\left(\frac{\partial W_r}{\partial y}\right)\right) ds \\
& \qquad\qquad (r=1, \cdots, n)
\end{aligned} \tag{9}
$$

where, q_i is the generalized coordinate. As the experiment was conducted with the frequencies ranging from 1 to 55 Hz and since there were three natural frequencies of the plate, the three degrees-of-freedom model was established. Furthermore, to consider the non-linear damping terms in Eq. (10), cubic non-linear damping terms (Ghanbari and Dunne, 1998; Doughty et al., 2003) and a quadratic term (Baker, 1961) were applied to Eq. (9).

$$
D = \alpha_{1i}\dot{q}_i + \alpha_{2i}\dot{q}_i q_i^2 + \alpha_{3i}\dot{q}_i^2 q_i + \alpha_{4i}\dot{q}_i|\dot{q}_i| \tag{10}
$$

Table 3 Parameters estimated via Continuous time identification

identified parameter	1st mode	2nd mode	3rd mode
α_{1i}	0.486×10^2	0.121×10^2	0.528×10^3
α_{2i}	6.622×10^6	4.008×10^6	2.896×10^6
α_{3i}	0.765×10^5	0.258×10^5	0.193×10^5
α_{4i}	0.207×10^3	0.026×10^3	0.394×10^3

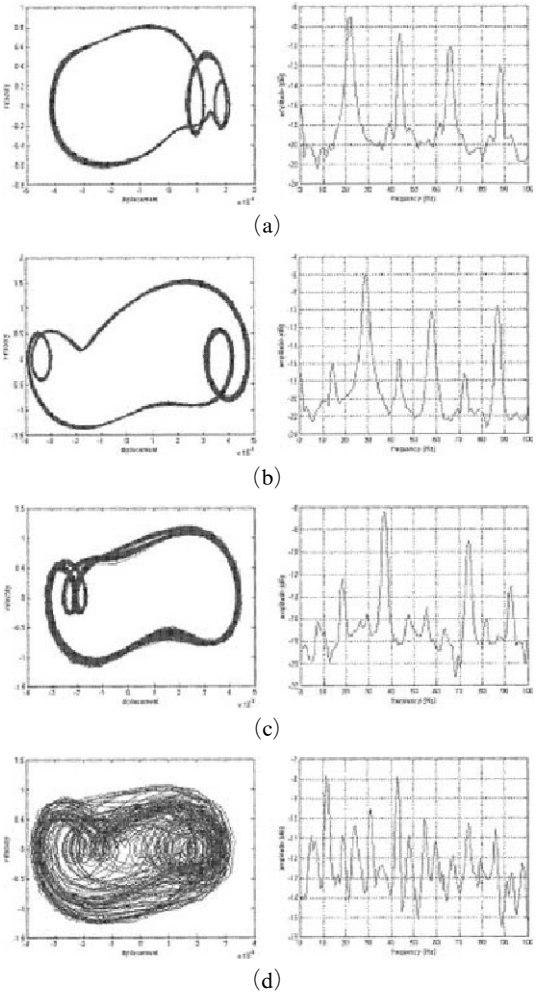

Fig. 11 Phase diagrams and power spectra of the first modal responses for ; (a) 22 Hz, (b) 29 Hz, (c) 37 Hz and (d) 55 Hz

Also, the unknown parameters of the non-linear terms can be estimated by continuous-time system identification technique (Ghanbari and Dunne, 1998) after having approximated, for the simplicity, the nonlinear equation of motion to each single mode (Kadiri and Benamar, 2003) as follows.

$$m_{ii}\ddot{q}_i+\alpha_{1i}\dot{q}_i+\alpha_{2i}\dot{q}_i q_i^2+\alpha_{3i}\dot{q}_i^2 q_i+\alpha_{4i}\dot{q}_i|\dot{q}_i| +k_{ii}q_i+2b_{iiii}q_i^3=W_i(x_0,y_0)F(t) \quad (11)$$

To estimate the unknown parameters with the experimental data, Eq. (11) was converted to the

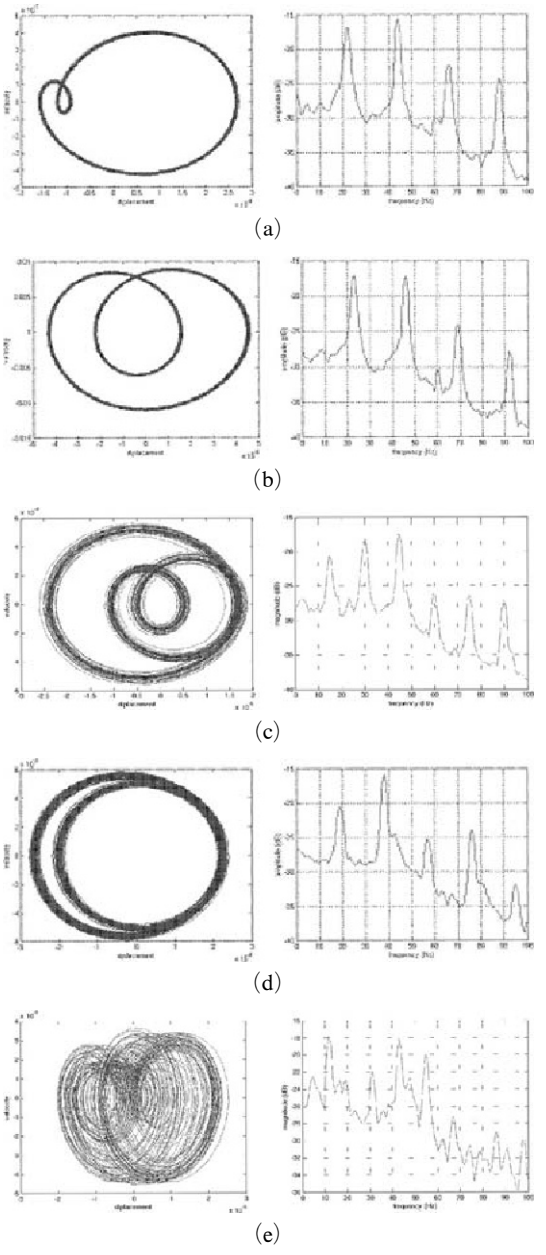

Fig. 12 Phase diagrams, power spectra of the second modal responses for ; (a) 21 Hz, (b) 22 Hz, (c) 30 Hz, (d) 37 Hz and (e) 55 Hz

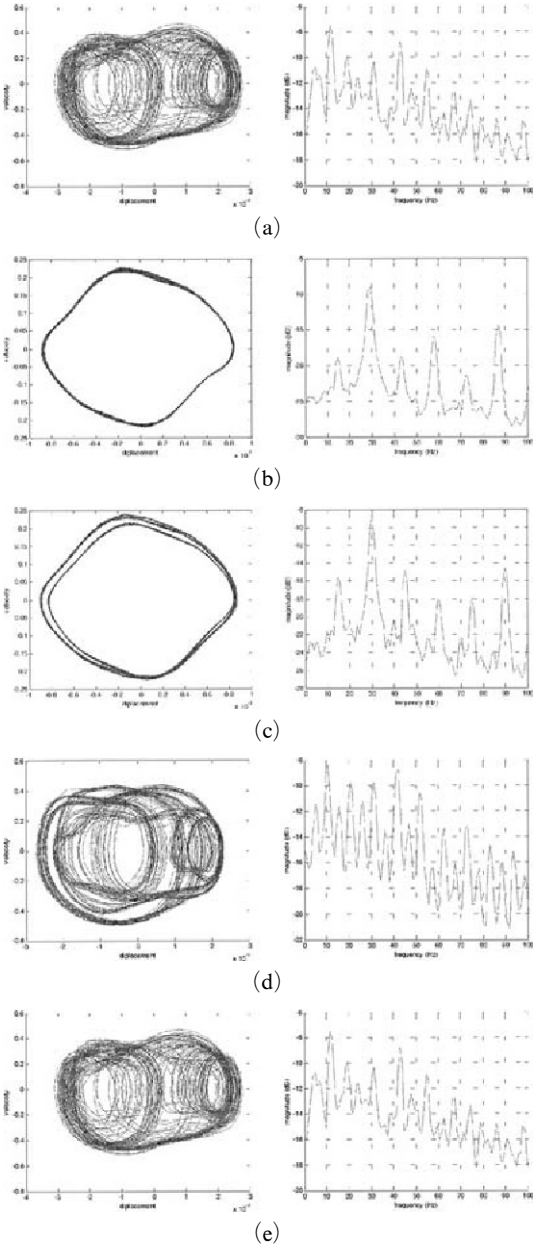

Fig. 13 Phase diagrams, power spectra of the third modal responses for ; (a) 22 Hz, (b) 29 Hz, (c) 30 Hz, (d) 52 Hz and (e) 55 Hz

matrix form of $K=A\cdot P$ as detailed in Eq. (12).

$$[m_{ii}\ddot{q}_i+k_{ii}q_i+2b_{iiii}q_i^3-W_i(x_0,y_0)F] = [-\dot{q}_i,-\dot{q}_iq_i^2,-\dot{q}_i^2q_i,-|\dot{q}_i|\dot{q}_i]\cdot\begin{bmatrix}\alpha_{1i}\\ \alpha_{2i}\\ \alpha_{3i}\\ \alpha_{4i}\end{bmatrix} \quad (12)$$

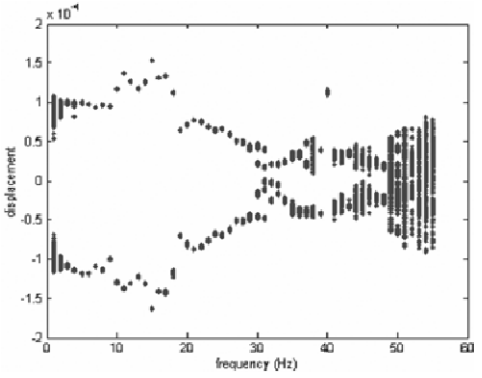

(a) The first mode

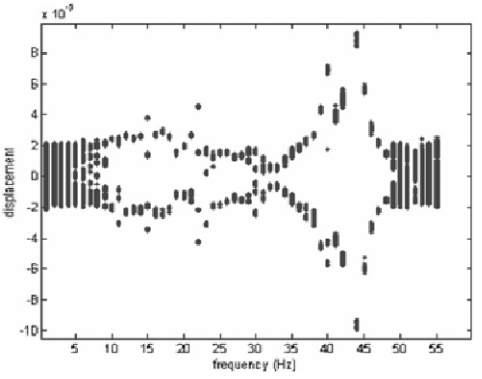

(b) The second mode

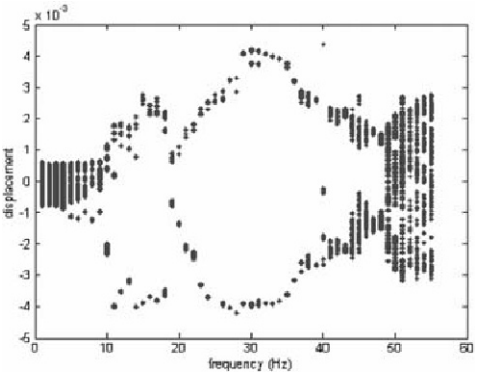

(c) The third mode

Fig. 14 Bifurcation diagram of the system by numerical analysis

where, K, A are the data from the experiments and P is the unknown parameters. The estimation results are shown in Table 3. Figs. 11 to 13 indicate the estimations of each mode in phase diagrams and power spectra. In Figs. 11 to 13, one can notice that the behavior of each modal displacement shows the two or more periodic motions by the subharmonic components and their multiple components as well as the chaotic motion that resulted. The bifurcation diagrams by the numerical analyses with the non-linear equation of motion are depicted in Fig. 14, and correlated with the experimental results.

4. Conclusions

In this study, the non-linear dynamic analyses of a plate were conducted experimentally and numerically. Considering the large deformation of the plate, the non-linear equation of motion was derived and non-linear damping terms were added in the equation. The parameters of the non-linear damping were estimated by a continuous-time system identification technique with a single mode approximation to the equation. The numerical results, which fitted with experimental results, were obtained. Consequently this study shows that the nonlinear parameters of a plate which is subject to a large deformation could be decided on the basis of experimental results.

References

Baker, W. E., etc., 1961, "Air and Internal Damping of thin Cantilever Beams," *International Journal of Mechanical Science*, Vol. 9. pp. 743～766.

Doughty, T. A., Davies, P. and Bajaj, A., 2003, "An Experimental Study of Parametrically Excited Cantilever Beam and System Identification of Nonlinear Modes," *ASME, Biennial Conference on Mechanical Vibration and Noise ; DETC2003*, pp. 2519～2528

Ghanbari, M. and Dunne J. F., 1998, "An experimentally Verified Non-Linear Damping Model for farge Amplitude Random Vibration of a Clamped-Clamped Beam," *Journal of Sound and Vibration*, Vol. 215, pp. 343～379.

Gorman, D. J., 1995, "Accurate Free Vibration Analysis of the Orthotropic Cantilever Plate," *Journal of Sound and Vibration*, Vol. 181, pp. 605～618.

Haterbouch, M. and Benamar, R., 2003, "The Effect of Large Vibration Amplitude on the Axisymmetric Mode Shapes and Natural Frequencies of Clamped thin Isotropic Circular Plates. Part 1 : Iterative and Explicit Analytical Solution for Non-Linear Transverse Vibrations," *Journal of Sound and Vibration*, Vol. 265, pp. 123～154.

Kadiri, M. E. and Benamar, R., 2003, "Improvement of the Semi-Analytical Method, Based on Hamilton's Principle and Spectral Analysis, for Determination of the Geometrically Non-Linear Response of thin Straight Structures. Part III : Steady State Periodic Forced Response of Rectangular Plates," *Journal of Sound and Vibration*, Vol. 264, pp. 1～35.

Kadiri, M. E., Benamar, R. and White, R. G., 1999, "The Non-Linear Free Vibration of Fully Clamped Rectangular Plates : Second Non-Linear Mode for Various Plate Aspect Ratios," *Journal of Sound and Vibration*, Vol. 228, No. 2, pp. 333～358.

Samtech, 2003, Samcef Field Manual, Samtech.

SMS, 1994, The Star System Manual, Spectral Dynamics, Inc.

Timoshenko, S. and Woinowsky-Kreiger, S., 1959, Theory of Plates and Shells, McGraw-Hill, New York.

Wong, W. O., 2002, "The Effects of Distributed Mass Loading on Plate Vibration Behavior," *Journal of Sound and Vibration*, Vol. 252, pp. 577～593.